Journal of the Earth and Space Physics, Vol. 44, No. 4, Winter 2019, P. 73-85
DOI: 10.22059/jesphys.2018.257443.1007005

Attenuation of spatial aliasing in CMP domain by non-linear interpolation of seismic data along local slopes

Khoshnavaz, M. J.[1*], Siahkoohi, H. R.[2] and Bóna, A.[3]

1. Post-Doc, Department of Earth Physics, Institute of Geophysics, University of Tehran, Iran
2. Professor, Department of Earth Physics, Institute of Geophysics, University of Tehran, Iran
3. Professor, Department of Exploration Geophysics, Curtin University of Technology, Perth, Western Australia

(Received: 14 May 2018, Accepted: 25 Sep 2018)

Abstract

Spatial aliasing is an unwanted side effect that produces artifacts during seismic data processing, imaging and interpolation. It is often caused by insufficient spatial sampling of seismic data and often happens in CMP (Common Mid-Point) gather. To tackle this artifact, several techniques have been developed in time-space domain as well as frequency domain such as frequency-wavenumber, frequency-space, and frequency-time. The main advantages of seismic interpolation in time-space domain over frequency domain are: a) frequency components of the initial signals are preserved, and b) the prior knowledge that a seismic event consists of many plane wave segments, can be used. Using the later advantage, a seismic event can be predicted by pursuing the continuity of seismic events in a trace-by-trace manner. This process, which has become popular in seismic data reconstruction and imaging within the past few years, is known as predictive painting. We use predictive painting to predict the wavefronts and two-way-travel time curves in regularly sampled CMP gathers followed by increasing the number of traces by cubic interpolation. Then, the amplitude of the interpolated trace is obtained by averaging the amplitudes of the neighbouring traces. Performance of the proposed method is demonstrated on several synthetic seismic data examples as well as a field data set.

Keywords: Spatial aliasing, interpolation, time-space, local slope, predictive painting.

1. Introduction

In exploration seismology, recorded seismic wavefront is the discretised version of the source generated continuous wavefront, where the spatial sampling is provided by the acquisition geometry. According to sampling theorem (Shannon, 1948) spatial aliasing occurs in regularly sampled data, when some of the constituent wavenumbers fall beyond the Nyquist wavenumber. These wavenumber components are folded back and appear lower than the Nyquist wavenumber. It leads to the contamination of unaliased part of the data with aliased one. Different factors may contribute to spatial aliasing such as large offsets, high frequency components, shallow reflectors, steeply dipping reflectors and low interval velocities (Claerbout, 1985; Yilmaz, 2001). Spatial aliasing widely affects seismic imaging by causing poor lateral resolution in final subsurface images (Spitz, 1991). A costly solution for spatial aliasing is to decrease sampling interval along spatial direction by increasing the receiver group interval during seismic acquisition; however, this solution might not be able to deal with under-sampled coherent artifacts (multiples), particularly in the areas where the artifacts have a much lower velocity than the primary energy (Gülünay, 2003).

A cost-effective alternative is the attenuation of spatial aliasing using signal processing/interpolation methods (Porsani, 1999; Zwartjes and Sacchi, 2007). According to Naghizadeh and Sacchi (2010), seismic data reconstruction/interpolation methods can be divided into two categories: wave-equation-based and signal-processing-based methods. The wave-equation-based methods use the physical concepts of the wave propagation and wavefront extrapolation. Such techniques require some prior knowledge of seismic velocities. Techniques developed by Ronen (1987), Stolt (2002), Fomel (2003), and Leggott et al. (2007) are classified under the wave-equation-based interpolation category. On the other hand, signal-processing techniques for interpolation/reconstruction of seismic data rely often on transformation of the data into

*Corresponding author: mj.khoshnavaz@ut.ac.ir

other domains. Such techniques include Radon transform (Lu, 1985; Turner, 1990; Trad et al., 2002; Sacchi et al., 2004; Yu et al., 2007; Wang et al., 2009; Ibrahim et al., 2015), curvelet transform (Herrmann and Hennenfent, 2008; Naghizadeh and Sacchi, 2010), wavelet-like/seislet transform (Liu and Fomel, 2010; Gan et al., 2015 and 2016), and shaping regularization techniques (Chen et al., 2015) relying on shaping/constraining operators in different transformation domains such as the sparsity-promoting and the Fourier transform. Another type of signal-processing-based interpolation method is established upon prediction error filtering (PEF) methods. These methods include PEF interpolation in frequency-space (*f-x*) domain (Spitz, 1991; Porsani, 1999; Trickett, 2003; Naghizadeh and Sacchi, 2007) and in frequency-wavenumber (*f-k*) domain (Gülünay, 2003).

Signal-processing-based interpolation techniques that rely on transformation of seismic data into other domains may face some problems. First, seismic transforms are not always reversible (e.g., Radon transform). In other words, direct and reverse transformation of the data (without any additional process) may result in the loss of some useful information. Second, frequency components of the original data may not be preserved. These potential limitations make the seismic interpolation techniques in *t-x* domain (Claerbout, 1992; Crawley, 2000; Fomel, 2002; Liu and Fomel, 2011) worthy of consideration and development. Local slope-based imaging, interpolation, and interpretation techniques, which are performed in *t-x* domain, are typically time-efficient and amplitude preservative (Fomel, 2007; Khoshnavaz et al., 2016a). This research aims to introduce a local slope-based nonlinear interpolation method using a numerical tool called "predictive painting".

Predictive painting, introduced by Fomel (2010), is a powerful prediction method in *t-x* domain, which is based on the prediction of each seismic event from its neighbouring traces that are shifted along local slopes. Its applications include seismic imaging (Khoshnavaz et al., 2016a; Khoshnavaz, 2017), seismic anisotropy (Burnett and Fomel, 2009; Casasanta and Fomel, 2011; Khoshnavaz et al., 2016b), and seismic interpretation (Karimi, 2015; Karimi et al., 2015). In this research, the predictive painting is employed to attenuate spatial aliasing in regularly sampled seismic data in CMP gather followed by increasing the number of samples using cubic interpolation. Then, the amplitudes of the neighbouring traces were averaged to build the new interpolated traces. The efficiency of the proposed approach is demonstrated on several synthetic seismic data examples as well as a field dataset.

2. Methodology

For the estimation of two-way-travel time (TWT) curves in the CMP domain, the predictive painting technique introduced by Fomel (2010) was used. The main idea behind the predictive painting is the prediction of each seismic event from its neighbouring traces that are shifted along the local slopes. Local slopes are estimated by computing the time-shift between two points of the same seismic wavefront. Given the local slopes, implementation of an inverse procedure gives the time-shift between the two neighbouring traces. The prediction procedure can be expressed by plane wave destruction (Claerbout, 1992; Fomel, 2002; Fomel et al., 2013). Plane wave destruction operation in the linear operator notation is expressed by Fomel (2010) as:

$$\boldsymbol{r} = \boldsymbol{D}(\sigma)\boldsymbol{s}, \tag{1}$$

where, σ is local slope, $\boldsymbol{s}$ denotes a window consisting of N traces ($[s_1 s_2 \dots s_N]^T$), $\boldsymbol{r}$ is the prediction error, and $\boldsymbol{D}$ is the destruction operator, defined as:

$$\boldsymbol{D} = \begin{bmatrix} \boldsymbol{I} & 0 & 0 & \cdots & 0 \\ -\boldsymbol{P}_{1,2}(\sigma) & \boldsymbol{I} & 0 & \cdots & 0 \\ 0 & -\boldsymbol{P}_{2,3}(\sigma) & \boldsymbol{I} & \cdots & 0 \\ \cdots & \cdots & \cdots & \cdots & \cdots \\ 0 & 0 & \cdots & -\boldsymbol{P}_{N-1,N}(\sigma) & \boldsymbol{I} \end{bmatrix}. \tag{2}$$

Herein, $\boldsymbol{I}$ denotes the identity operator and $\boldsymbol{P}_{i,j}(\sigma_i)$ denotes a prediction operator that predicts trace j from trace i. The prediction of trace $\boldsymbol{s}_k$ from a reference trace $\boldsymbol{s}_r$ can be defined by $\boldsymbol{P}_{r,k}\boldsymbol{s}_r$, where

$$\boldsymbol{P}_{r,k} = \boldsymbol{P}_{r,k}, \dots, \boldsymbol{P}_{r+1,r+2}\boldsymbol{P}_{r,r+1}. \tag{3}$$

In Equation (3), $\boldsymbol{P}_{r,k}$ expresses the predictive operator. Following the same concept, Khoshnavaz et al. (2016a, 2016b) described the travel time predictive operator as:

$$t_{r-k} = t_r - \left(\sum_{m=0}^{k-1} \sigma_{x_{r-m}}\right)\Delta x, \quad (4)$$

Where, Δx denotes receiver spacing.

As mentioned in the previous section, predictive painting is a powerful numerical tool that can be used in several areas of seismic data processing and interpretation. In this research, this numerical tool was used to attenuate special aliasing in CMP gather by nonlinear interpolation of seismic events along local slopes. Since the predictive painting has the ability of connecting more than two points of a seismic event, it gives more information about the curvature or nonlinearity of the seismic events. An outline of the interpolation procedure conducted in this research is summarized as:

- Implementation of predictive painting from zero- to longest offset for all the events in a CMP gather,
- Extraction of all TWT curves in the gather
- Increasing the number of samples by the application of cubic interpolation along each estimated TWT curve
- Averaging amplitudes of the original neighbouring samples and substituting the corresponding results to the new/interpolated samples.

Analogous to Burnett and Fomel (2009), Casasanta and Fomel (2011), and Khoshnavaz et al. (2016b), the whole wavefront from the zero- to maximum offsets was predicted. It is also possible to divide the whole offset to smaller segments and to apply the above steps in each segment (Fomel, 2010).

3. Synthetic data examples

3-1. Single linear event

In this example, seismic interpolation using predictive painting is applied to a synthetic dataset including a single linear event generated by convolutional modelling. In this example and also the following synthetic examples, a Ricker wavelet with dominant frequency of 20 Hz was used. Figure 1a shows the corresponding gather decimated by the factor of two. Figure 1b shows the *f-k* spectrum of the decimated gather, which indicates the existence of spatial aliasing.

In CMP gather, one can take advantage of the prior knowledge of dip orientation. As an example, dip orientations are either positive or negative in a CMP gather of an off-end survey. In a spatially aliased CMP gather, there are two types of dips: true and aliased dips. The mentioned prior knowledge of dip orientation helps to avoid wrong estimation of dips. Figure 1c shows the estimated dips by the application of plane wave destructor (Fomel, 2002). As mentioned in the previous section, the whole recorded wavefront from the zero to maximum offsets was considered for predictive painting. Figure 1d illustrates the corresponding zero-offset TWTs estimated by the application of predictive painting.

Given the estimated zero-offset TWTs, one can extract the TWT curves using the fact that TWTs with the same zero-offset TWT belong to the same seismic wavefront. The procedure of predicting TWT curves from the predicted zero-offset TWTs is known as time-warping (Burnett and Fomel, 2009). Figures 1e-1f show the corresponding time-warp spectrum, and comparison between the exact and the predicted TWT curve for the liner event with the zero-offset intercept time of 0.4 s. In order to have a better recognition of the estimated attributes at different time horizons, the local slopes, zero-offset TWT and time-warp spectra were filtered out in the areas where there was no data.

Given the predicted TWT curves, we increased the number of samples using cubic interpolation, although using cubic and linear interpolations gives the same results in this example, since there is only a single linear seismic event. The amplitudes of the neighbouring traces were averaged and utilized to construct the new interpolated traces. Figures 1g to 1i show the interpolated section, its *f-k* spectrum and the amplitude residual between the original and interpolated data, respectively. It is observed that the spatial aliasing has been removed and there is almost no amplitude residual. It is due to the fact that there was only a single dipping event in the data; hence, uncertainty in the estimation of the local slopes is minimal.

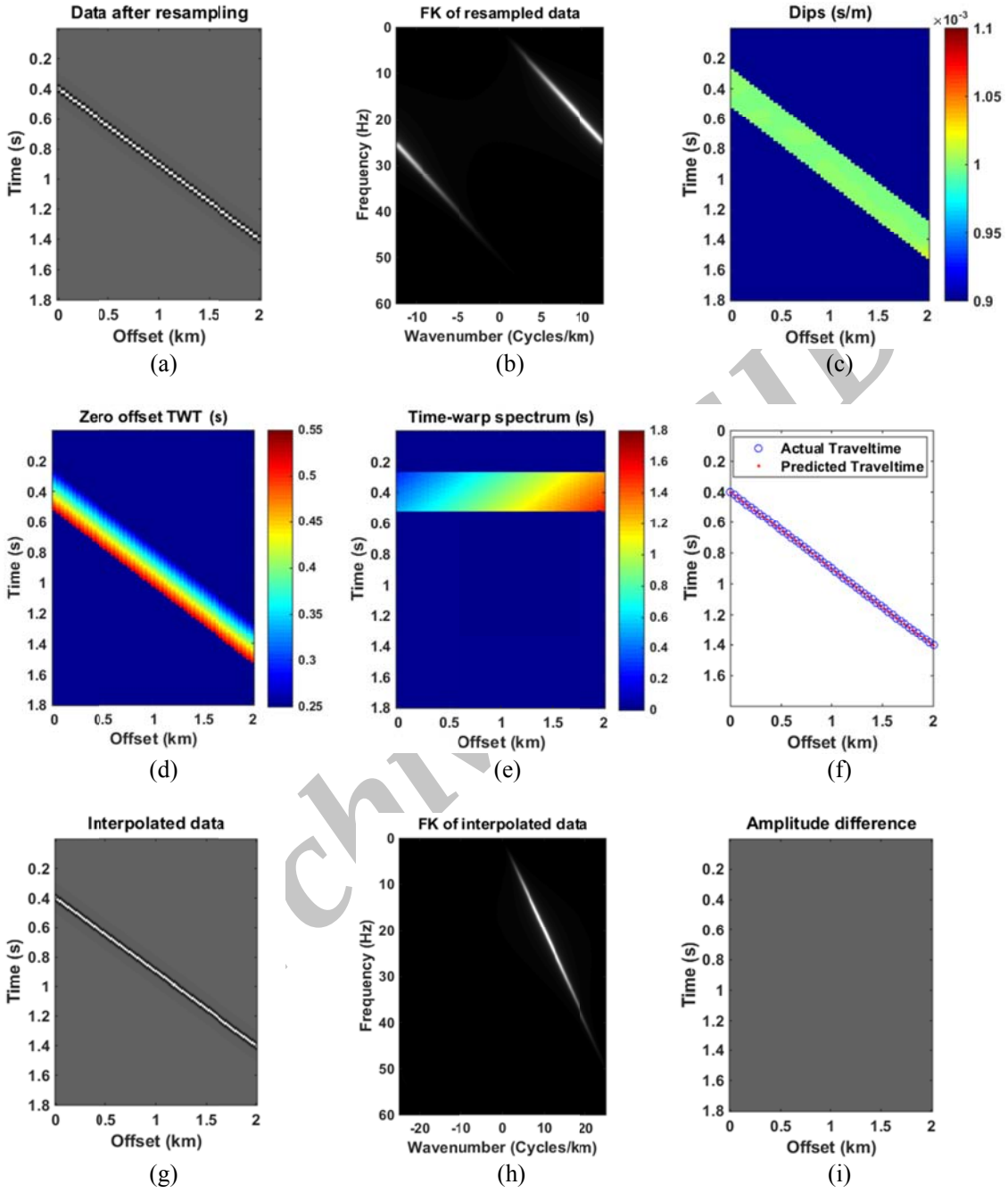

Figure 1. a) Synthetic data after decimation by the factor of two. b)f-k spectrum of data in (a), c) local slopes of data in (a) by plane wave destructor, d) zero-offset TWT estimated by predictive painting, e) time –warp spectrum of data in (a). f) comparison between the traveltime used for forward modelling and the predicted traveltime curve by predictive painting for the liner event with the intercept time of 0.4 s on data in (a). g) interpolated data, h) f-k spectrum of data in (g) and i) the amplitude difference between the original data and the interpolated data.

3-2. CMP gather with nonlinear events

In this example, the presented interpolation technique is applied to a synthetic CMP gather including several nonlinear events. Figure 2a shows the CMP gather decimated by the factor of two along offset axis. Figure 2b shows the *f-k* spectrum of the decimated CMP gather, which indicates the presence of spatial aliasing. This paper followed the same workflow used for the interpolation of seismic data in the previous example. Figures 2c to 2e show the dips estimated by plane wave destructor, estimated zero-offset TWT by the predictive painting and the estimated TWT curves using time-warping, respectively. To quantify the accuracy of the predicted TWTs, the exact TWT curve with zero-offset intercept time of 0.95 s was compared with its predicted TWT curve in Figure 2f. Note that time-warping faces the "stretch" problem in the area of shallower events at far offsets (similar to NMO stretch). It results in discontinuous TWT curves in time-warp spectrum. In order to deal with this, cubic interpolation was applied along the offset axis for each time-warp spectra in all the examples presented in this paper. Figures 2g to 2i show the interpolated section, its *f-k* spectrum and the corresponding amplitude residual between the original and the interpolated data, respectively. Spatial aliasing was removed but the amplitude difference is not as negligible as it was in the previous example. This was expected to happen because of dip variation within the CMP gather.

3-3. Sensitivity to noise

Accuracy of all local slope-based signal processing, imaging and inversion techniques depends on the accuracy of the estimated local slopes. Plane wave destructor is less sensitive to white/band-limited noise comparing to the other local slope estimation techniques that use numerical differentiation (Khoshnavaz et al., 2016a). This is because plane wave destructor relies on smoothing and regularisation of seismic data (Fomel, 2002); however, when signal-to-noise ratio (S/N) is very low, the precision of the estimated local slopes by plane wave destructor followed by the final interpolation results will also be affected.

To evaluate the performance of the interpolation technique in the presence of noise, the synthetic CMP gather used in the previous example was contaminated with band-limited noise with the frequency content of 5-150 Hz so that the S/N was 10 (Figure 3a). This level of S/N is fairly acceptable for the residual noise left in a gather/section after pre-processing and denoising (Chen et al., 2014). Equation (5) was used to scale the S/N.

$$\frac{S}{N} = \frac{E_S}{E_N} = \frac{\sum_{i=1}^{n}\sum_{j=-m}^{m} {A_S}_{i,j}{}^2}{\sum_{i=1}^{n}\sum_{j=-m}^{m} {A_N}_{i,j}{}^2}, \quad (5)$$

where A_S and A_N denote the amplitude of signal and noise at each data sample, respectively. Indices i and j denote trace and sample number for each data sample within the windowed seismic event ($2m$), respectively. Figure 3b shows the *f-k* spectrum of the decimated noisy CMP gather that indicates the presence of spatial aliasing. Figures 3c to 3e illustrate the dips estimated by plane wave destructor, estimated zero-offset TWT using predictive painting, and the estimated TWT curves using time-warping, respectively. Figure 3f compares the accuracy of the predicted TWTs and the exact TWT curve with zero-offset intercept time of 0.95 s.

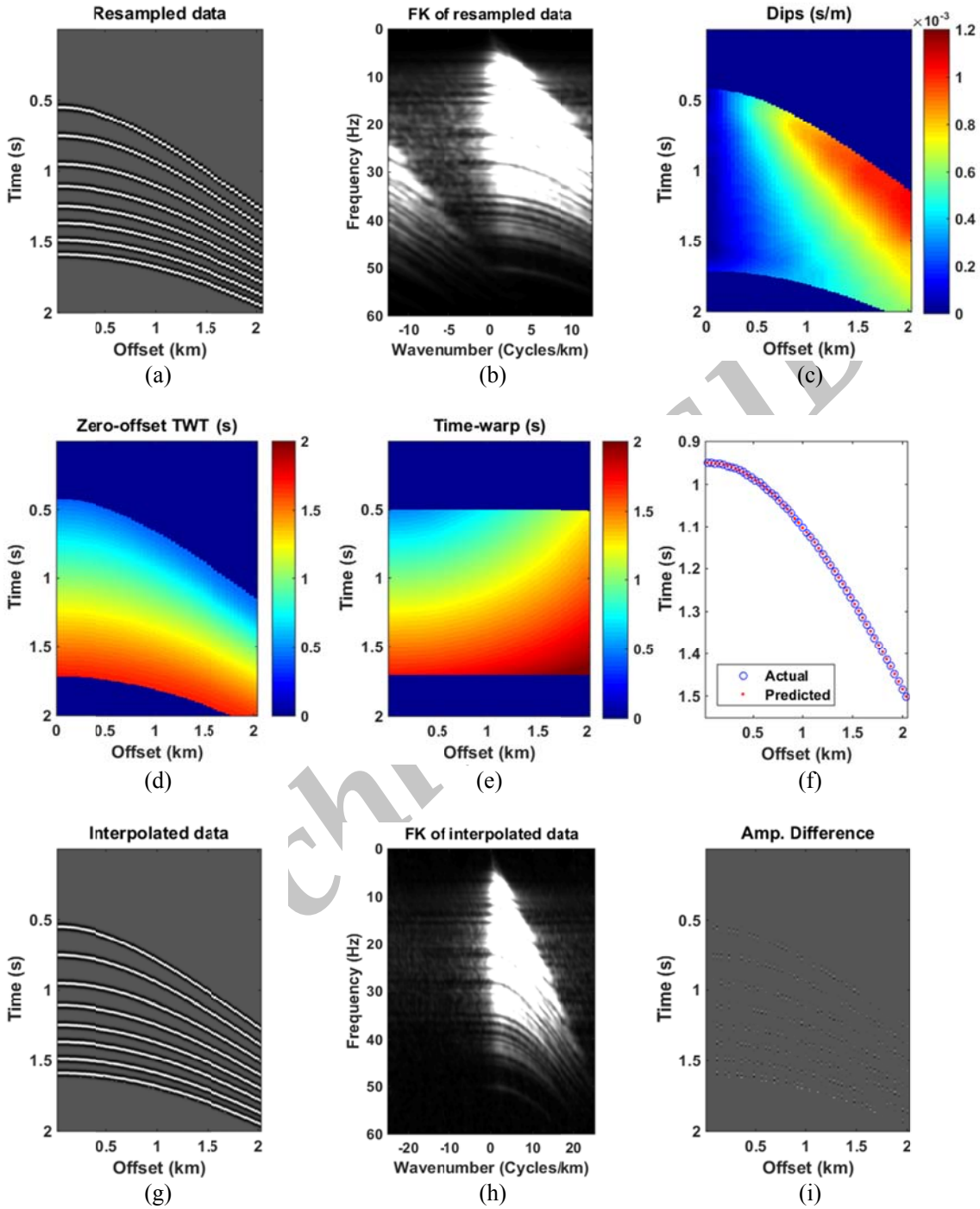

Figure 2. a) Synthetic CMP gather after decimation by the factor of two, b)f-k spectrum of data in (a), c) local slopes of data in (a) by plane wave destructor, d) zero-offset TWT estimated by predictive painting, e) time–warp spectrum of data in (a), f) comparison between the exact TWT curve and the predicted TWT curve by predictive painting for the event with the intercept time of 0.95 s on data in (a), g) interpolated data, h)f-k spectrum of data in (g) and i) the amplitude difference between the original data and the interpolated data.

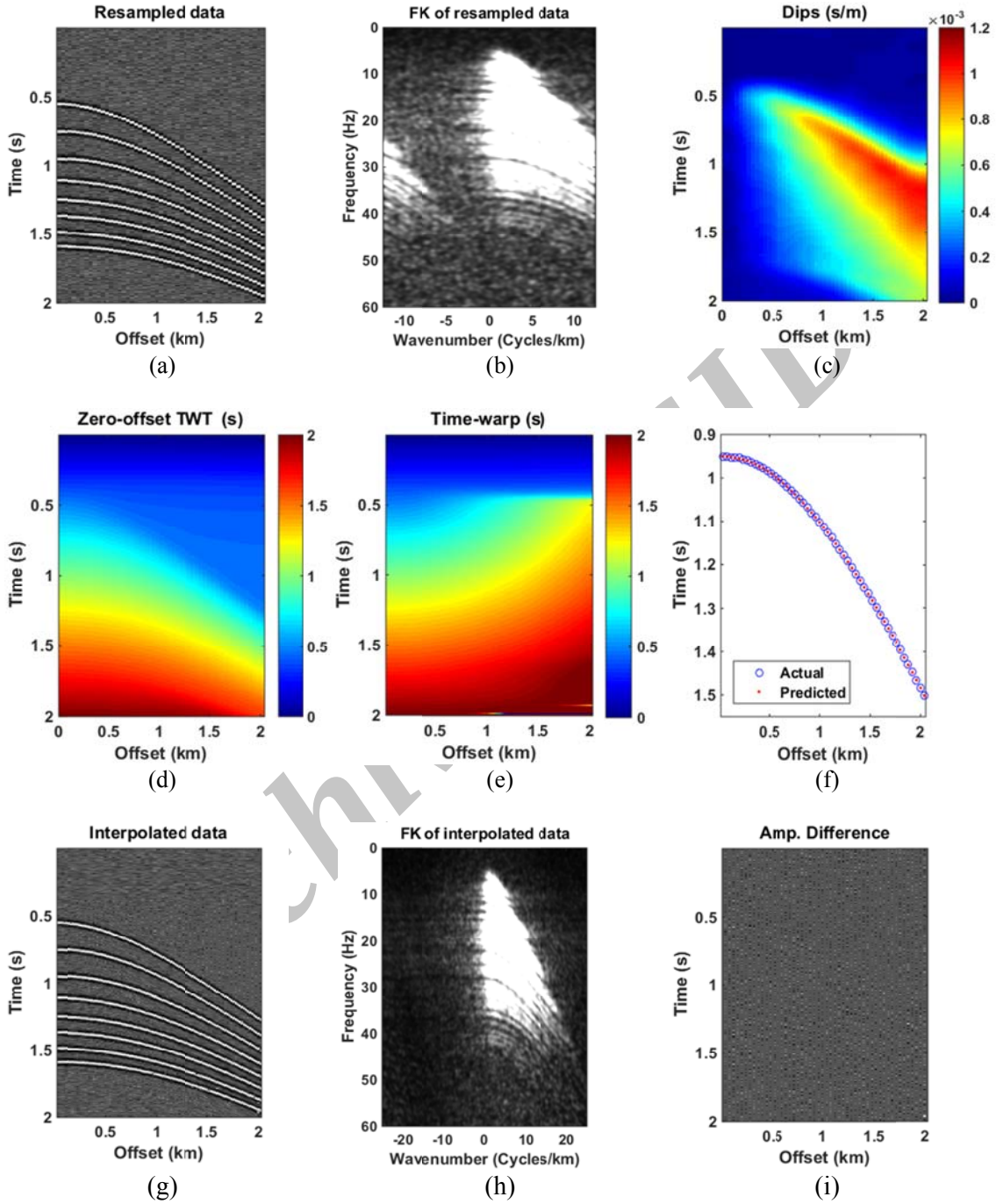

Figure 3. a) Decimated synthetic CMP gather of Figure (2a) contaminated with band-limited white noise (S/N=10) , b)f-k spectrum of data in (a), c) local slopes of data in (a) by plane wave destructor, d) zero-offset TWT estimated by predictive painting, e) time–warp spectrum of data in (a), f) comparison between the exact TWT curve and the predicted TWT curve by predictive painting for the event with the intercept time of 0.95 s on data in (a), g) interpolated data, h)f-k spectrum of data in (g) and i) the amplitude difference between the original data and the interpolated data.

4. Field data example

In this example, the interpolation technique was applied on a marine CMP gather provided by Geoscience Australia. Figure 4a shows the CMP gather decimated by the factor of two. Figure 4b shows the *f-k* spectrum of the decimated marine CMP gather expressing the presence of spatial aliasing. This example followed the same workflow used for the interpolation of the synthetic seismic data examples. Figures 4c to 4e show the estimated local slopes/dips, zero-offset TWTs, and TWT curves by time-warping, respectively. Figure 4f shows several predicted TWT curves indicated by the red lines that are plotted on top of the decimated CMP gather. One can see that the predicted curves follow the seismic trends.

Figures 4g to 4i illustrate the interpolated CMP gather, the corresponding *f-k* spectrum and the amplitude residual between the initial and the interpolated marine CMP gathers, respectively. As can be seen, spatial aliasing is highly attenuated with a negligible amplitude residual.

5. Discussion

The performance of de-aliasing by nonlinear interpolation of seismic data in CMP domain was studied on several synthetic and field data examples that did not contain conflicting events/dip. The results were acceptable as the amplitude differences between the original un-decimated data and the interpolated data were not considerable. The question is: how well does the interpolation technique work in the presence of conflicting events? In principle, it should be misdirected at the location of the intersections of the events where there is more than a single dip. Here, a feasibility study was done by applying the interpolation technique on a CMP gather containing several conflicting events. The CMP gather decimated by the factor of two along the spatial axis is shown in Figure 5a. The corresponding *f-k* spectrum is shown in Figure 5b, indicating the existence of spatial aliasing.

The corresponding estimated dips, zero-offset TWTs, and the time-warp spectrum are shown in Figures 5c to 5e, respectively. Figure 5f shows the main predicted TWT curves indicated by the different colours over laid the CMP gather. It confirms our expectation about the occurrence of misdirection during the predictive painting. We stepped further and applied the interpolation technique on the CMP gather using the over and/or under-estimated TWT curves.

Figures 5g to 5i show the results of interpolation, the corresponding *f-k* spectrum and the amplitude difference between the initial and the interpolated data, respectively. The results show that the interpolation technique by the predictive painting surprisingly works. The amplitude difference is negligible among the whole section except at the location of some intersections. The explanation is the predicted TWT curves cover the whole section and since the technique relies on the interpolation of each seismic trace from its neighbouring traces, all the section is interpolated.

To predict TWT curves, the whole recorded wavefront from the zero- to maximum offsets was used. The error in prediction of the curves might be minimized by applying the predictive painting locally. It can be done by dividing the whole offset into smaller portions followed by the implantation of the predictive painting on each individual portion. It is the subject to test as the future of the presented work.

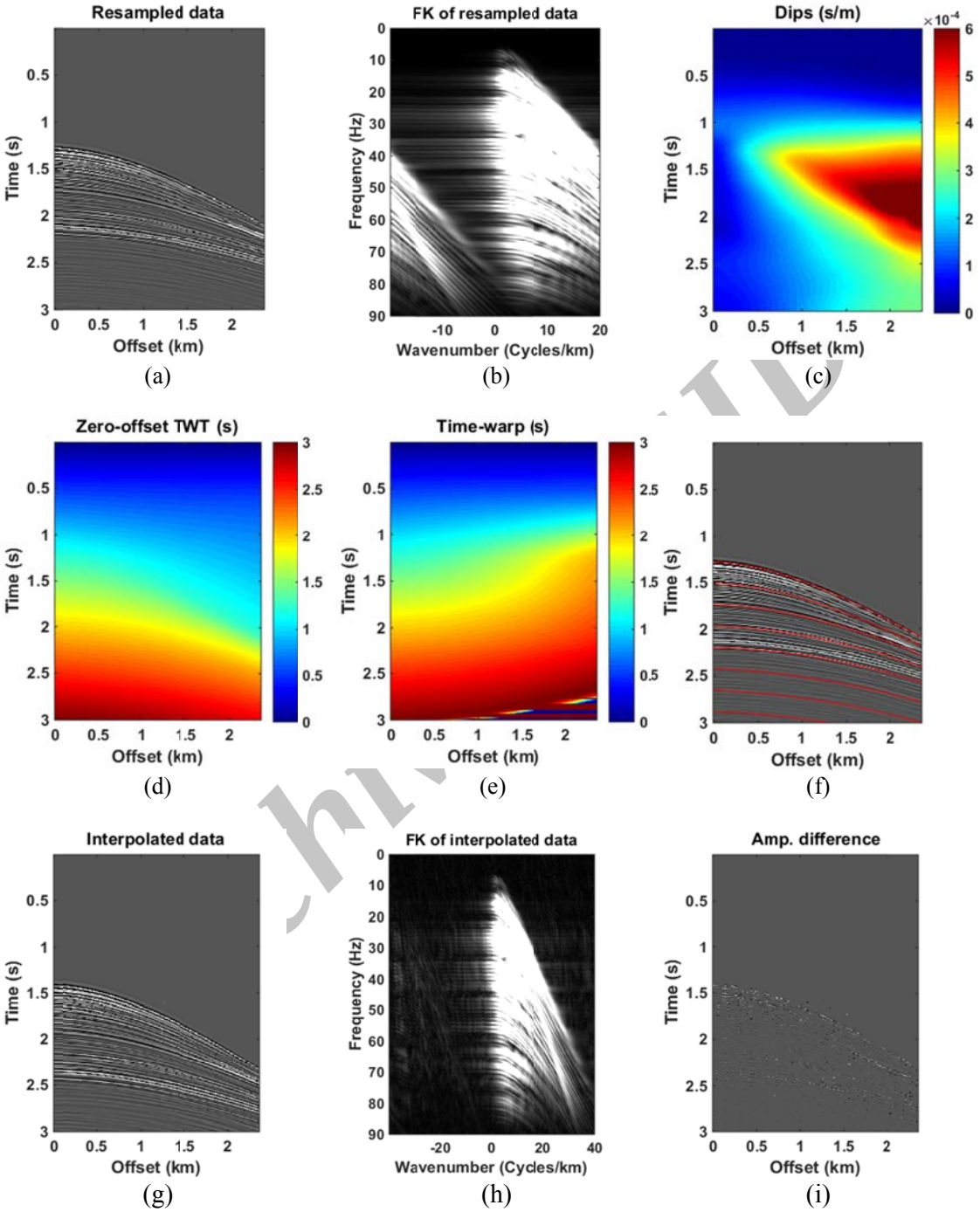

Figure 4. a) A marine CMP gather after decimation by the factor of 2 , b)f-k spectrum of data in (a), c) local slopes of data in (a) by plane wave destructor, d) zero-offset TWT estimated by predictive painting, e) time–warp spectrum of data in (a), f) several TWT curves (red lines) estimated by predictive painting for events on data in (a), g) interpolated data, h)f-k spectrum of data in (g) and i) the amplitude difference between the original data and the interpolated data.

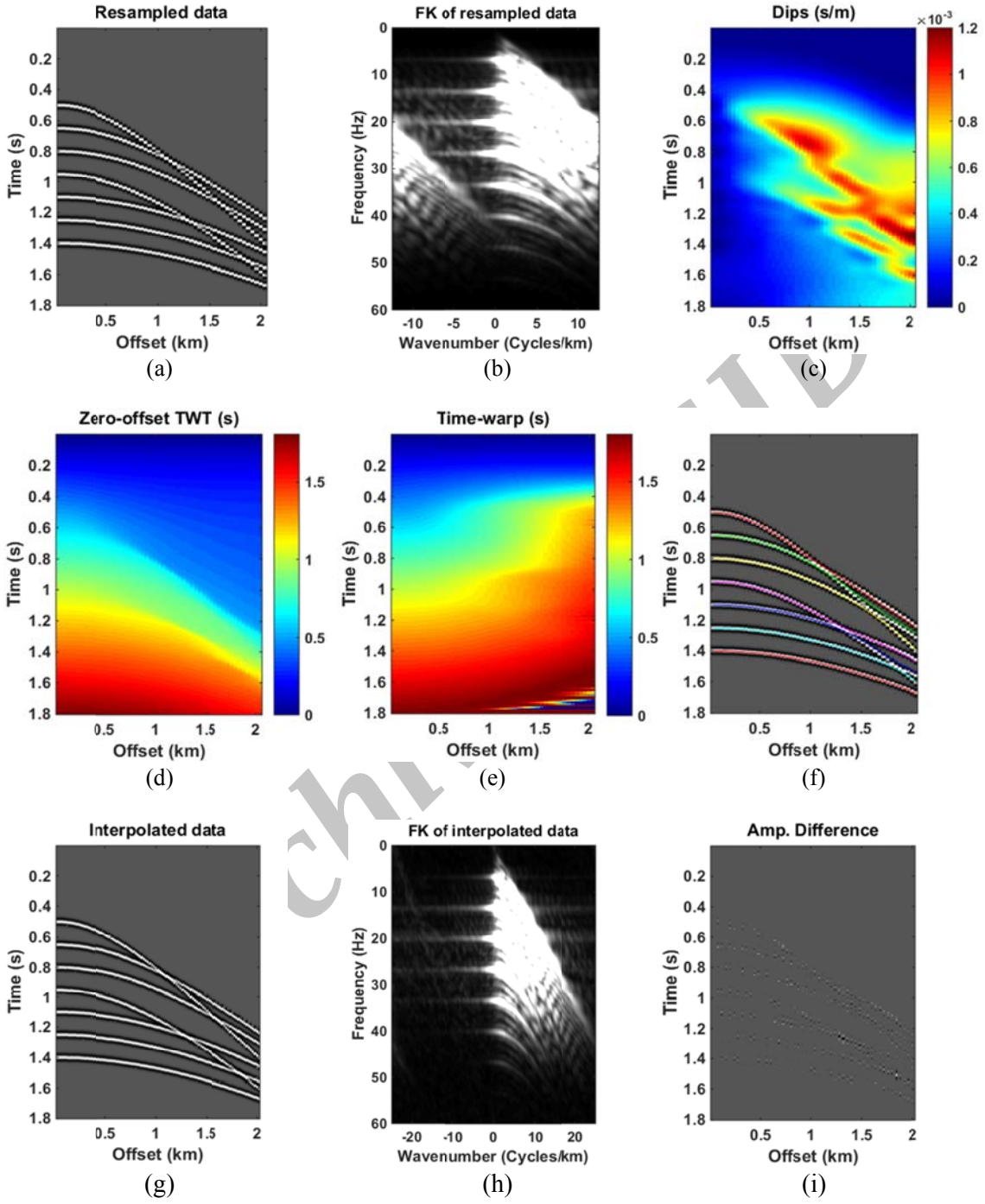

Figure 5. a) A Synthetic CMP gather including conflicting events, after decimation by the factor of two, b)f-k spectrum of data in (a), c) local slopes of data in (a) by plane wave destructor, d) zero-offset TWT estimated by predictive painting, e) time–warp spectrum of data in (a), f) the main predicted curves plotted on top of decimated data in (a), g) interpolated data, h)f-k spectrum of data in (g) and i) the amplitude difference between the original data and the interpolated data.

6. Conclusion

Predictive painting is a powerful tool in the estimation of TWT of seismic events, dominantly in time-space domain. It has become popular in the area of seismic imaging, seismic anisotropy and seismic interpretation within the past few years. This paper employed the predictive painting for the attenuation of spatial aliasing in CMP domain by non-linear interpolation of seismic data along local slopes. The performance of the proposed interpolation technique was demonstrated on several synthetic data examples and a field marine CMP gather. Since the presented workflow is time-efficient and frequency-independent, it can be used as an alternative technique for seismic data interpolation, specifically for offshore data that does not contain considerable level of noise. The road ahead is to employ the presented technique for seismic data extrapolation.

Acknowledgements

Authors would like to acknowledge Geoscience Australia for providing the marine data. The authors would also like to acknowledge Madagascar Open-Source Project for providing the multidimensional data analysis package.

References

Bóna, A., 2011, Shot-gather time migration of planar reflectors without velocity model. Geophysics, 76(2), S93–S101, doi: 10.1190/1.3549641.

Burnett, W. and Fomel, S., 2009, 3D velocity-independent elliptically anisotropic move out correction. Geophysics, 74(5), WB129–WB136, doi: 10.1190/1.3184804.

Casasanta, L. and Fomel, S., 2011, Velocity-independent τ-p move out in a horizontally layered VTI medium. Geophysics, 76(4), U45-U57, doi: 10.1190/1.3595776.

Chen, Y., Fomel, S. and Hu, J., 2014, Iterative deblending of simultaneous-source seismic data using seislet-domain shaping regularization. Geophysics, 79, V183-V193, doi: 10.1190/GEO2013-0449.1.

Chen, Y., Zhang, L. and Mo, L., 2015, Seismic data interpolation using nonlinear shaping regularization. Journal of Seismic Exploration, 24(5), 327-342, http://www.geophysical-press.com/contents_jse_vol_24_4.htm.

Claerbout, J. F., 1985, Imaging the Earth's Interior. Blackwell Scientific Publications, Inc., http://sepwww.stanford.edu/sep/prof/iei2.

Claerbout, J. F., 1992, Earth Soundings Analysis: Processing Versus Inversion. Blackwell Scientific Publications, http://sepwww.stanford.edu/sep/prof/pvi.pdf.

Crawley, S., 2000, Seismic trace interpolation with nonstationary prediction error filters: Ph.D. thesis, Stanford University.

Fomel, S., 2002, Applications of plane-wave destruction filters. Geophysics, 67, 1946–1960, doi: 10.1190/1.1527095.

Fomel, S., 2003, Seismic reflection data interpolation with differential offset and shot continuation. Geophysics, 68, 733–744, doi: 10.1190/1.1567243.

Fomel, S., 2007, Velocity-independent time-domain seismic imaging using local event slopes: Geophysics, 72(3), S139–S147, doi: 10.1190/1.2714047.

Fomel, S., 2010, Predictive painting of 3D seismic volumes. Geophysics, 75(4), A25–A30, doi: 10.1190/1.3453847.

Fomel, S., Sava, P., Vlad, I., Liu, Y. and Bashkardin, V., 2013, Madagascar: open-source software project for multidimensional data analysis and reproducible computational experiments. Journal of Open Research Software, 1(1), p. e8, doi: oftware.metajnl.com/articles/10.5334/jors.ag/

Gan, S., Wang, S., Chen, Y., Jin, Z. and Zhang, Y., 2015, Dealiased Seismic Data Interpolation Using Seislet Transform With Low-Frequency Constraint, IEEE Geoscience and Remote Sensing Letters, 12, 2150-2154, doi: 10.1109/LGRS.2015.2453119.

Gan, S., Chen, Y., Wang, S., Chen, X., Huang, W. and Chen, H., 2016, Compressive sensing for seismic data reconstruction using a fast projection onto convex sets algorithm based on the seislet transform. Journal of Applied Geophysics, 130, 194-208, doi:

10.1016/j.jappgeo.2016.03.033.

Gülünay, N., 2003, Seismic trace interpolation in the Fourier transform domain. Geophysics, 68, 355–369, doi: 10.1190/1.1543221.

Herrmann, F. J. and Hennenfent, G., 2008, Non-parametric seismic data recovery with curvelet frames: Geophysical Journal International, 173(1), 233–248, doi: 10.1111/j.1365-246X.2007.03698.x.

Ibrahim, A., Terenghi, P. and Sacchi, M. D. , 2015, Wavefield Reconstruction using a Stolt-Based Asymptote and Apex Shifted Hyperbolic Radon Transform: 55th Annual International Meeting, SEG, Expanded Abstracts, 3836-3841, doi: 10.1190/segam2015-5873567.1.

Karimi, P., 2015, Structure-constrained relative acoustic impedance using stratigraphic coordinates. Geophysics, 80(3), A63–A67, doi: 10.1190/GEO2014-0439.1.

Karimi, P., Fomel, S., Wood, L. and Dunlap, D., 2015, Predictive coherence: Interpretation, 3(4), SAE1–SAE7, doi: 10.1190/INT-2015-0030.1.

Khoshanavaz, M. J., Bóna, A., Urosevic, M., Dzunic, A. and Ung, K., 2016a, Oriented prestack time migration using local slopes and predictive painting in common-source domain for planar reflectors. Geophysics, 81(6), S409–S418, doi: 10.1190/GEO2016-0127.1.

Khoshanavaz, M. J., A. Bóna, and Urosevic, M., 2016b, Velocity-independent estimation of kinematic attributes in vertical transverse isotropy media using local slopes and predictive painting. Geophysics, 81(5), U73-U85, doi: 10.1190/GEO2015-0638.1.

Khoshnavaz, M. J., 2017, Oriented time-domain dip move out correction for planar reflectors in common-source domain. Geophysics, 82(6), U87-U97, doi: 10.1190/geo2016-0577.1

Leggott, R. J., Wombell, R., Conroy, G., Noss, T. and Williams, G., 2007, An efficient least-squares migration: 69th Conference and Exhibition, EAGE, Expanded Abstracts, P178, doi: 10.3997/2214-4609.201401856.

Liu, Y. and Fomel, S., 2010, OC-seislet: Seislet transform construction with differential offset continuation. Geophysics, 75(6), WB235–WB245, doi: 10.1190/1.3479554.

Liu, Y. and Fomel, S., 2011, Seismic data interpolation beyond aliasing using regularized nonstationary auto regression. Geophysics, 76(5), V69–V77, doi: 0.1190/GEO2010-0231.1.

Lu, L., 1985, Application of local slant-stack to trace interpolation: 55th Annual International Meeting, SEG, Expanded Abstracts, 560–562, doi: 10.1190/1.1892818.

Naghizadeh, M. and Sacchi, M. D. , 2007, Multistep autoregressive reconstruction of seismic records. Geophysics, 72(6), V111–V118, doi: 10.1190/1.2771685.

Naghizadeh, M. and Sacchi, M. D., 2010, Beyond alias hierarchical scale curvelet interpolation of regularly and irregularly sampled seismic data. Geophysics, 75(6), WB189–WB202, doi: 10.1190/1.3509468.

Porsani, M., 1999, Seismic trace interpolation using half-step prediction filters. Geophysics, 64, 1461–1467, doi: 10.1190/1.1444650.

Ronen, J., 1987, Wave-equation trace interpolation. Geophysics, 52, 973–984, doi: 10.1190/1.1442366.

Sacchi, M. D., Verschuur, D. J. and Zwartjes, P. M., 2004, Data reconstruction by generalized deconvolution: SEG, Expanded Abstracts, 23, 1989–1992, doi: 10.1190/1.1843303.

Shannon, C. E., 1948, A Mathematical Theory of Communication: Bell System Technical Journal, 27(3), 379–423, doi:10.1002/j.1538-7305.1948.tb01338.x.

Spitz, S., 1991, Seismic trace interpolation in the F-X domain. Geophysics, 56, 785–794, doi: 10.1190/1.1443096.

Stolt, R. H., 2002, Seismic data mapping and reconstruction. Geophysics, 67, 890–908, doi: 10.1190/1.1484532.

Trad, D., Ulrych, T. J. and Sacchi, M. D., 2002, Accurate interpolation with high-resolution time-variant Radon transforms. Geophysics, 67, 644–656, 10.1190/1.1468626.

Trickett, S. R., 2003, F-xy eigenimage noise suppression. Geophysics, 68, 751–759, doi: 10.1190/1.1567245.

Turner, G., 1990, Aliasing in the τ-p transform and the removal of spatially

aliased coherent noise. Geophysics, 55, 1496–1503, doi: 10.1190/1.1442797.

Wang, J., Ng, M. and Perz, M., 2009, Fast high-resolution Radon transforms by greedy least-squares method. SEG, Expanded Abstracts, 28, 3128–3132, doi: 10.1190/1.3255506.

Yilmaz, O., 2001, Seismic data analysis. SEG, doi: 10.1190/1.9781560801580.

Yu, Z., Ferguson, J., McMechan, G. and Anno, P., 2007, Wavelet-Radon domain dealiasing and interpolation of seismic data. Geophysics, 72(2), V41–V49, 10.1190/1.2422797.

Zwartjes, P. M. and Sacchi, M. D. , 2007, Fourier reconstruction of nonuniformly sampled, aliased seismic data. Geophysics, 72(1), V21–V32, doi: 10.1190/1.2399442.